Title	Coping with electrode polarization for development of DC-driven electrical impedance tomography
Author(s)	Hirose Yoshiyasu, Sagawa Jun, Shibamoto Yasuteru, Kukita Yutaka
Citation	Flow Measurement and Instrumentation,81,p.102006_1- 102006_9
Text Version	Published Journal Article
URL	https://jopss.jaea.go.jp/search/servlet/search?5071115
DOI	https://doi.org/10.1016/j.flowmeasinst.2021.102006
Right	

Flow Measurement and Instrumentation 81 (2021) 102006

Contents lists available at ScienceDirect

Flow Measurement and Instrumentation

journal homepage: www.elsevier.com/locate/flowmeasinst

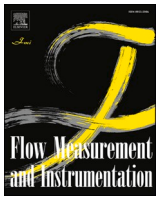

Coping with electrode polarization for development of DC-Driven electrical impedance tomography

Yoshiyasu Hirose [a,*], Jun Sagawa [b], Yasuteru Sibamoto [a], Yutaka Kukita [a]

[a] Japan Atomic Energy Agency, 2-4, Shirakata, Tokai, Ibaraki, 319-1195, Japan
[b] Mito Electric Solution, Inc. 879-9-301, Moto-Yoshida-cho, Mito, Ibaraki, 310-0836, Japan

ARTICLE INFO

Keywords:
Electrical impedance tomography (EIT)
Two-phase flow
Electrode polarization
Pulsed-DC injection
Four electrode system

ABSTRACT

An electrical impedance tomography (EIT) system design is proposed for imaging of phase distribution in gas-water two-phase flow from boundary measurement of electrical potentials in response to direct current (DC) injection. DC injection simplifies substantially the system design, but introduces problems due to polarization of injection electrodes. Electrode polarization means charge accumulation on the electrode-water interface causing a drift in the interfacial potential difference. The polarization problems are coped with by using dedicated electrodes for injection and potential measurement, and using a current source unaffected by the polarization of current-carrying electrodes (CCEs). Furthermore, the polarization of CCEs is controlled, to lessen the possible influence on the sensing electrodes (SEs), by using a short (milliseconds in width) pulse for injection with a charge balanced injection strategy. The impact of electrode polarization and the effectiveness of countermeasures introduced in the present design are discussed through comparisons of measured boundary potentials and of images reconstructed for a simple object simulating large bubbles in water.

1. Introduction

Electrical Impedance Tomography (EIT) is a non-invasive, radiation-free imaging method that reconstructs the conductivity distribution of an object inversely from boundary measurement of electrical potential pattern for given current injection density. EIT is easy to implement and applicable basically irrespective of the size of object (measurement field). Its accuracy, however, is limited due to the severe ill-posedness of the inverse conductivity problem [1], and is sensitive to the quality of potential measurement on boundary electrodes. Typical spatial resolution is 3–10% of the object diameter [2] while efforts are made for enhanced resolution with improved electrode design [3], reconstruction algorithm [4], and machine learning [5].

Practical application of EIT technique has been active in medical, geophysical, and civil engineering fields as a tool for diagnostics, survey and monitoring of, e.g., lung ventilation [6], natural landslides [7], and moisture transport in cementitious materials [8]. There is a growing interest in application to multiphase flows related to industrial processes. Attempts made so far for gas/liquid two-phase flows include flow regime identification [9], phase boundary detection in separated flow [10,11] and phase distribution measurement in dispersed flow [12]. In these applications, at least part of electrode surfaces is in contact with water containing dissolved electrolyte.

The great majority of existing and proposed EIT systems in literature use alternating current (AC) for injection, despite that many of them concern the resistivity distribution, rather than impedance, in the object, as is the case for two-phase flow measurement. While the AC methods have evolved to produce improved versions for advanced measurements based on e.g., multifrequency excitation [13] and frequency dependence of permittivity [14], the methods require complicated setups for relatively-high frequency signal processing including demodulation, even for simplest designs. Direct current (DC)-driven systems can be much simpler and can be built with a smaller number of parts available at reasonable costs.

The main reason for the limited use of DC injection appears to be the concerns about electrode polarization [15,16]. Electrode polarization refers to charge accumulation in an electrical double layer (EDL) that forms on the interface between the electrode and electrolyte solution, and associated changes in the potential difference across the interface. These occur inevitably when current is injected through metallic 'polarizable' electrodes. Polarization occurs for both AC and DC injections, but in different manners. For an AC injection, polarization is

* Corresponding author.
E-mail address: hirose.yoshiyasu@jaea.go.jp (Y. Hirose).

https://doi.org/10.1016/j.flowmeasinst.2021.102006
Received 10 March 2021; Received in revised form 31 May 2021; Accepted 30 June 2021
Available online 6 July 2021

observed mainly as finite impedance across the electrode interface (termed 'contact impedance' or 'polarization impedance') dependent on the frequency of injected current. The polarization with DC injection is characterized by that the charge accumulation grows with time of injection, and the charge remains in the EDL after the injection is turned off, taking time to be resolved [15,16]. Electrode polarization matters when it hampers measurement of potential differences for a given injection current, while it may pose additional, safety-related problems in medical applications.

Four-electrode measurement technique, with use of a pair of sensing electrodes (SEs) separately from the current-carrying electrode (CCE) pair, provide means for measurement of potential difference unaffected by the CCE polarization for both AC and DC driven systems [17,18]. For the technique to be effective, the sensing amplifier should have input impedance much higher than the object impedance to be measured and a high common mode rejection ratio (CMRR). It is desirable that CCEs and SEs are dedicated ones to avoid the possible influence of residual polarization of CCEs on measurements. Furthermore, the current source needs to be unaffected by the CCE polarization.

Measurement for EIT needs to be taken for a number of current injection patterns to obtain one frame of data for reconstruction. The time spent for each pattern hence should be short and seems to range from tens of microseconds to milliseconds in existing designs except those which focus on impedance characteristic at low frequencies [14]. For each pattern, current is injected as a discrete pulse through assigned CCEs. In AC-driven designs, each pulse consists of many cycles of sinusoidal waves, for which the mean amplitude of the responding potential is measured through frequency-domain signal processing. If resistivity, rather than impedance, is to be measured, however, the injected current does not need to be pulsed sinusoidal. Instead, a singe square shaped unipolar or bipolar pulse can be used for injection to enable the potential to be measured as a DC signal. Designs that take this approach are called DC-driven in the present paper.

The current amplitude should be large enough for producing potential difference signals with a high signal to noise ratio. For DC-driven systems, the amplitude should be low enough, at the same time, to keep the electrode potentials (the potential difference between the CCEs minus the voltage drop in water) below the values for which faradaic reactions become significant even after repeated injections. It is not difficult to limit the increase in the electrode potentials when the duration of each current injection (pulse width) is small. Nevertheless, bipolar, charge-balanced injection strategy can be taken for limiting the development of CCE polarization. This strategy is effective also in coping with offsets appearing in potential measurements as will be discussed in Section 2.4.

The basic specifications of an EIT system design presented in this paper are summarized in Table 1.

This paper is organized as follows. Section 2 describes the electrode design and the influences of electrode polarization that should be cope with. Section 3 presents the EIT system design. Section 4 describes the method and selected results of image reconstruction conducted for design validation. Finally, Section 5 presents our conclusions.

Table 1
Basic design specifications.

Items	Values
Current pulse amplitude	200–500 μA
Current pulse width	1–5 ms
Potential difference to be measured	0.1–1 V
Number of electrode units	16

2. Electrode design and performance

2.1. Electrode design

The present design uses 16 strip-shaped electrode units placed equidistantly on the periphery of a 97-mm i.d. test vessel. No systematic design guidelines seem to exist regarding the EIT electrode structure or parameters, although it has been pointed out that the electrode width and spacing, as well as the number, affect the sensitivity and spatial resolution [3]. The units used in the present design are 6 mm wide and about 13 mm spaced apart from each other. As a result, the electrode surfaces cover about 31.5% of the vessel peripheral length.

Each unit has a compound structure consisting of 6 SEs and one CCE. Each SE is a 2 mm × 3 mm rectangular island electrode encircled by the CCE with a 1 mm spacing as shown in Fig. 1. This spacing is enough to keep SEs unaffected by the polarization of CCE as will be shown. The second SE from the bottom is used in the experiments results from which are presented in this paper. All the electrodes are made of gold-plated copper.

2.2. Polarization of current carrying electrodes (CCEs)

We have explored the polarization behavior of CCEs by conducting experiments for both realistic and extreme conditions. The injection condition for the latter ranged up to 5 s in pulse width and 1000 μA in current amplitude. Some data taken for realistic injection conditions for EIT experiments in the geometry shown in Fig. 2 are presented in this subsection.

The measurement configurations are shown in Fig. 3 by using equivalent circuit models. In this subsection the CCE polarization behavior is discussed by comparing data taken by two-electrode method (Fig. 3(a)) with four-electrode data taken for the particular configuration shown in Fig. 3(b) where injection and measurements are made using the same pair of electrode units (Unit 1 and Unit 3 in Fig. 2(a)).

In the equivalent circuits shown in Fig. 3, each CCE-water interface is modeled by a parallel RC circuit $C_p||R_p$. The capacitance C_p represents the capacitance of an EDL on the interface, and the resistance R_p represents the sum of charge transfer resistance and diffusion resistance. The RC model is an oversimplified representation of electrode polarization, although it serves as a basis for more sophisticated modeling.

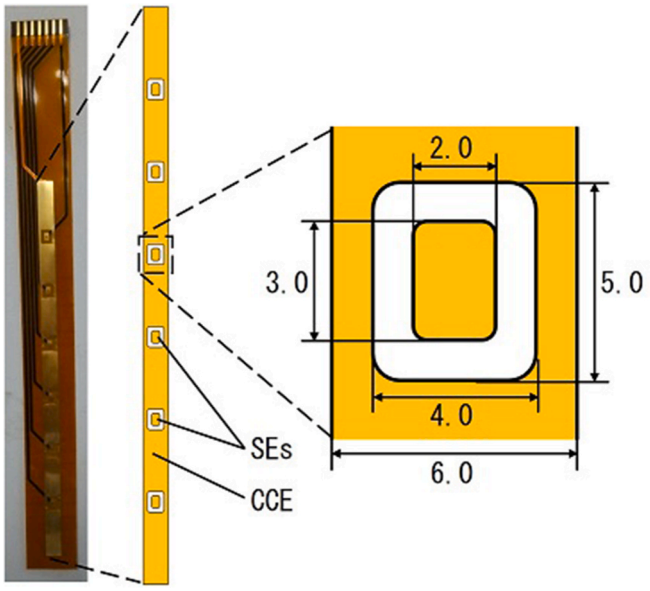

Fig. 1. Electrode design. Left: photo of an electrode unit. Center: schematic drawing of an electrode unit. Right: enlarged view of one of the sensing electrodes. (Unit: mm).

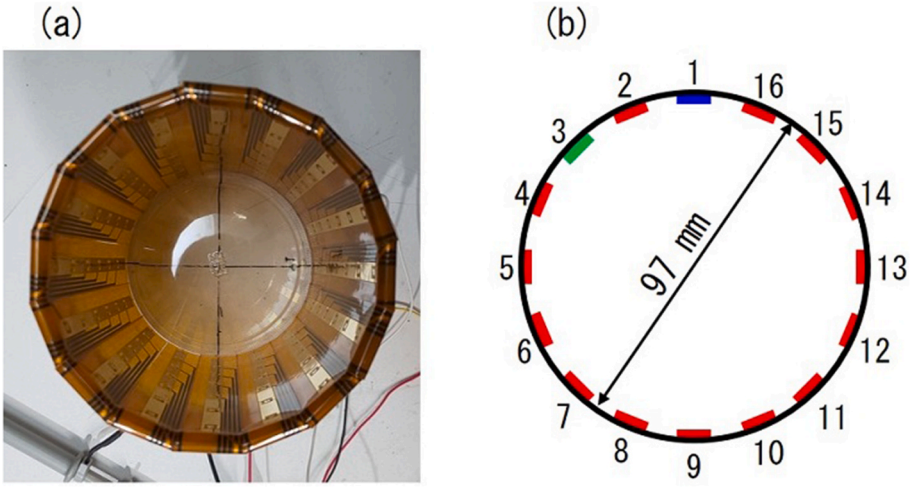

Fig. 2. Top view of EIT geometry. (a) photo of experimental setup with sixteen electrode units attached on the inner wall of a cylindrical vessel. (b) schematic drawing of electrode arrangement. Data shown in this subsection were taken by using Unit 1 (blue) and Unit 3 (green) each for both injection and measurement. (For interpretation of the references to colour in this figure legend, the reader is referred to the Web version of this article.)

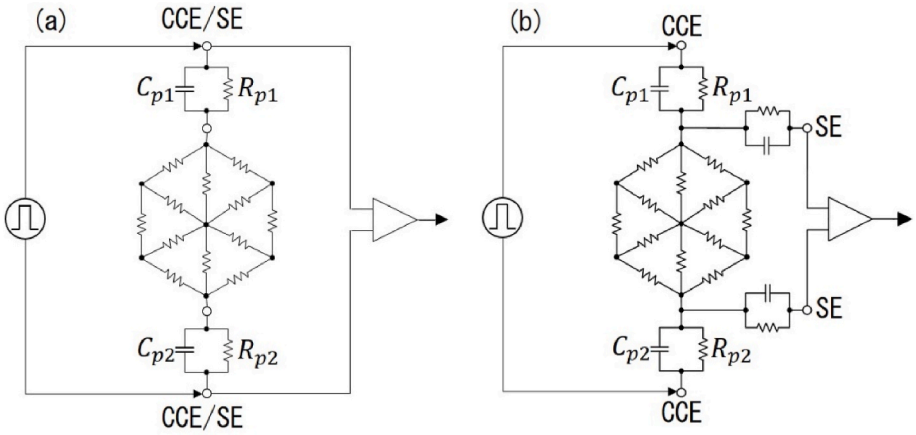

Fig. 3. Equivalent circuits for (a) two-electrode method and (b) four-electrode method. The water resistance between the driven CCEs is represented by a resistor network.

Fig. 4 shows two-electrode data, ΔE_2, and four-electrode data, ΔE_4, taken for a 100 Hz bipolar square-pulse injection with an amplitude of 200 μA, for the configurations shown in Fig. 2. The half-cycle pulse width, 5 ms, is longer than the standard pulse width of 1 ms for EIT measurements, while the pulse amplitude is within the range indicated in Table 1. The results in Fig. 4 therefore somehow exaggerate the magnitude of CCE polarization that would occur in actual EIT measurements.

The two-electrode data (black line in Fig. 4(b)) represents the total potential difference between the two CCEs where a stepwise increase, from negative to positive, in the injected current is imposed at a time defined to be 0 ms. The response of potential difference consists of a stepwise increase due to the liquid resistance, and a subsequent nonlinear increase reflecting the polarization of the two CCEs connected in series.

The injected current (Fig. 4(a)) has a clean square-pulse waveform, owing to the use of a constant current source (an enhanced Howland current pump), built with an Analogue Devices unit-gain amplifier AMP03. From comparison with the two-electrode potential waveform, it is seen that the current source well accommodates the nonlinear, capacitive response of its load.

The four-electrode measurement of the water potential difference, ΔE_4 (blue line in Fig. 4(b)), nearly replicates the waveform of injected current, basically unaffected by the CCE polarization, despite that the SEs used here were only 1 mm apart from the active CCEs.

For this configuration (Fig. 3(b)), with negligibly small water resistance between each SE and enclosing CCE, the difference between the two-electrode and four-electrode potential, $\Delta E_{2-4} = \Delta E_2 - \Delta E_4$ (green line in Fig. 4(b)) provides the sum of interfacial potential differences of the two CCEs (working as anode and cathode). Stated differently, it provides the difference between the anodic and cathodic potentials measured relative to a certain reference electrode, $\Delta E_{2-4} = \Delta E_{anode} - \Delta E_{cathode}$.

The four-electrode method is evidently advantageous for measurement of potential response to DC pulse injections. The problems of the two-electrode method are discussed briefly in the following based on the experimental results.

In Fig. 3(a), the two-electrode measurement configuration is represented by a parallel-series circuit

$$C_{p1}||R_{p1} + R_w + C_{p2}||R_{p2} \tag{1}$$

where R_w is the water resistance between the active electrodes. The response of this circuit to a stepwise change of current at $t = 0$ ms, with a peak-to-peak amplitude ΔI, to a final value I is given by a bi-exponential decay function

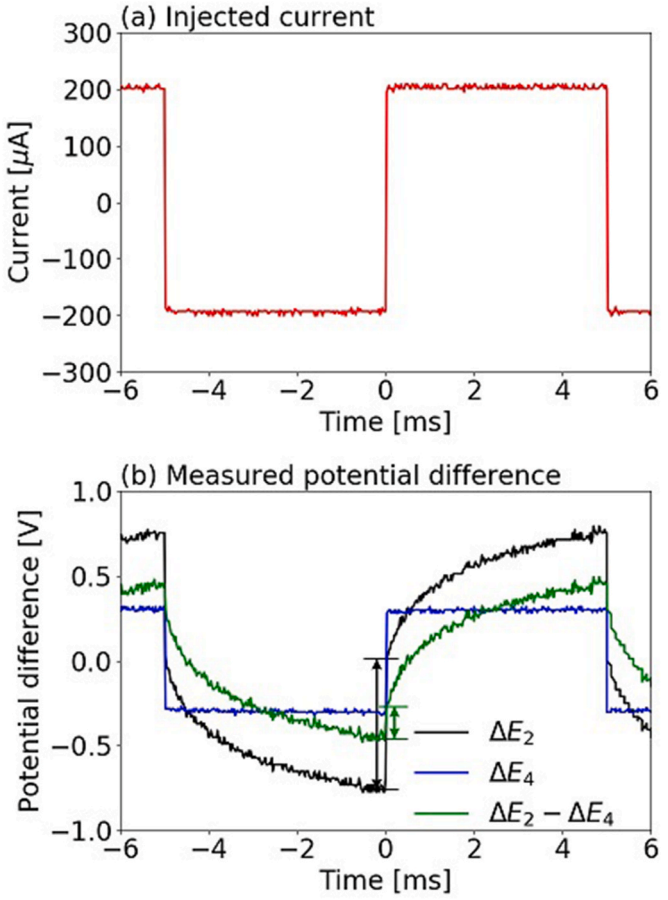

Fig. 4. Two- and four-electrode data taken for a 100 Hz bipolar square-pulse injection with an amplitude of 200 μA (a) Waveform of injected current. (b) Waveforms of two-electrode data ΔE_2 (black line), four-electrode data ΔE_4 (blue line), and the difference between them ΔE_{2-4} (green line). The vertical double arrows indicate *iR* drop-like changes in potential differences. (For interpretation of the references to colour in this figure legend, the reader is referred to the Web version of this article.)

$$\Delta E_2(t) = a\left[\exp\left(-\frac{t}{R_{p1}\,C_{p1}}\right)-1\right] + I\,R_w + b\left[\exp\left(-\frac{t}{R_{p2}\,C_{p2}}\right)-1\right] + \Delta E_2(-0) \tag{2}$$

The values of a and b depend on the magnitude of polarization of respective electrodes such that $a = I\,R_{p1} - \Delta E_{anode}(-0)$, $b = I\,R_{p2} - \Delta E_{cathode}(-0)$, and therefore, depend on the current injection history up to $t = 0$ ms.

According to the solution (Eq. (2)) for the equivalent circuit model Fig. 3(a), the stepwise change in ΔE_2 seen in Fig. 4(b) upon the current reversal ($t = 0$ ms) would be interpreted as the resistive voltage drop (so called *iR* drop) [19] in water between the two CCEs, $\Delta I\,R_w$, where ΔI is the peak-to-peak amplitude of the current leading edge. If so, this portion of two-electrode waveform could be regarded as potential difference unaffected by CCE polarization. However, in reality, ΔE_{2-4} also indicates a small stepwise change at that moment, showing that the EDL response to a fast current transient is not purely capacitive. Therefore, the *iR* drop-like change in ΔE_2 should not be taken, at least strictly speaking, to be equal to, or proportional to the resistive voltage drop in water.

While the ΔE_2 waveform after the stepwise change looks like a constant-current charge up of a parallel-series RC circuit given by Eq. (2), or more simply by $E = (E_0 - I\,R)\exp(-t/C\,R) + I\,R$, the reality is more complicated. Curve fitting using constant values of R and C, or a constant time constant $\tau = R\,C$, as proposed in Ref. [20] for correction of polarization effect, does not work well. Although fitting may be done alternatively by introducing a constant phase element or like that [21], the fitting parameter values would change depending on the amounts and composition of water impurities that are difficult to control in EIT applications.

Hence, the use of two-electrode data either by extracting the *iR* drop-like potential change, or correcting for the polarization effect, does not seem recommendable.

The approach taken in the present design is to practically eliminate the influence of CCE polarization on potential measurement by using dedicated SEs in four-electrode method and dedicated CCEs driven by a constant current source. Nevertheless, it is desirable to limit the magnitude of CCE polarization because the increase in CCE-water potential difference prompts faradaic reactions involving water impurities. This can result in CCE surface contamination and changes in nearby ion concentration that can affect the performance of SE belonging to the same unit. The use of low-amplitude, short pulses for current injection well suites this purpose.

2.3. Polarization of passive electrodes

The conducting surfaces of electrodes attached to the object boundary can deform the electrical field to be measured. This effect, known as the shunting effect, has been considered in EIT algorithms for AC-driven systems by taking account of finite contact impedance between the object and electrode surfaces [22]. The contact impedance reflects the electrode polarization in response to the imposed electrical field, i.e., the potential gradient along the electrode surface. The contact impedance takes small values per contact area at frequencies used in AC-driven systems, because the EDL capacitance is known to be ~10 μF/cm2. This means that the shunting effect, reducing the amplitude of potential difference, will be significant in AC-driven systems. In DC-driven systems the shunting effect may be observed as capacitive deformation of potential difference waveform similar to what is called "induced" polarization in geophysical EIT applications [23]. The induced polarization is thought to be caused by charge transport and accumulation in underground heterogeneous materials in response to electric field.

The four-electrode data shown in Fig. 4 were taken for adjacent-but-one injection/measurement arrangement shown in Fig. A1 with which the potential gradient along the passive electrode is maximized for a given current amplitude. The influence of frequency and configuration on the waveform of potential difference has been studied experimentally as summarized in Appendix A. The results show that capacitive response appears only in such cases where the interference by a conducting surface on the electrical field between the SEs is further strengthened. The waveform distortions observed in actual EIT measurement were within the range that the measurement protocol described in Section 3 can accommodate.

2.4. Polarization of sensing electrodes (SEs)

EIT systems generally suffer from offsets in the potential measurements [24]. The offsets are attributed to unreleased charges at certain locations in the measurement circuitry including the electrode used for measurement. In the present design we use dedicated SEs to avoid the influence of charge accumulation on CCEs, and use instrumentation amplifiers with high input impedance ranging from 10^{10} to 10^{12} ohm (typ) and low input bias current ranging from ±50 to ±500 pA (typ). Still, non-negligible offsets have been observed when measurements were carried out for a long time, and there is possibility that polarization of SEs due to the bias current cause such offsets. Another possibility is faradaic reactions on active CCEs cause changes in nearby ion concentration that affect the half-cell potential of SEs close to those CCEs. This may possibly occur when current is purposely injected repeatedly into a

fixed pair of CCEs as in experiments where data presented in Section 2.2 and Appendix A were taken.

Based on these experiences and considerations, an injection-measurement timing sequence, shown in Section 3, has been developed for obtaining offset-corrected potential difference data.

3. EIT setup and performance test

Fig. 5 shows schematically the electrode connections. The CCEs are connected to a constant current supply, and the SEs are connected to a single-channel measurement circuitry, through respective multiplexers (MUXs). Both the combination of electrodes and the polarity of connection are chosen by the four MUXs following the injection and measurement protocols.

The timing and duration of current injection are controlled by analogue switches timed with the MUXs and data acquisition. The control logic takes care of offsets in measured signals. Offsets have been observed also in existing (mostly AC driven) EIT systems posing difficulties for fast measurements [24]. To address this problem, a four-step procedure is taken for injection and measurement as shown in Fig. 6. Every time after the MUXs select a combination of CCEs and SEs, the analogue switches and measurement circuitry are directed to (1) withhold injection and wait for a user specified time (e.g., 1 ms), (2) measure the potential difference between the selected SEs and record it as V_1, (3) start injection between the selected CCEs and wait for a user specified time (e.g., 1 ms), and then (4) measure the potential difference again and record it as V_2. The influence of offsets can be eliminated by using the net change in potential difference in response to the injection, $V_2 - V_1$, for reconstruction. The waiting times could be shortened to what is really needed for signal settling while the present design places priority on robust measurement.

It is desirable that EIT systems and components be easily testable. Testing of electrodes would be important particularly when their surfaces are not accessible easily for cleaning. An intuitive way of fault detection is available by simply displaying signals obtained for a homogeneous object, e.g., vessel or piping filled with water, using the fact that 'normal' signals from such measurements indicate pseudo-periodical patterns dependent on injection-measurement strategies. Fig. 7 shows an example of such data display. The data shown here were obtained for a measurement configuration shown by an equivalent circuit in Fig. 3. Each data point was obtained by injection and measurement between the same pair of electrode units: with injection ($m \rightarrow n$) and measurement (m, n), where $1 \leq m, n \leq 16$). The measured potential differences are plotted against an index $16 \times (n - 1) + m$. The four-electrode data (red lines) indicate a repetition of bell-shaped changes, since the distance between the units changes almost cyclically, becoming zero when $|m - n| = 0$ and maximizing when the two units are opposed to each other, $|m - n| = 8$. (The changes are interrupted by minute plateaus that occur where m and n vary at the same time, from $[m = 16, n = N]$ to $[m = 1, n = N + 1]$, keeping the distance

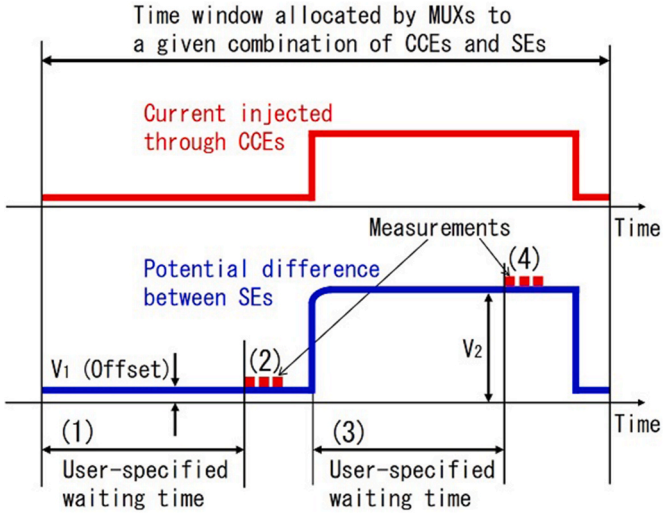

Fig. 6. Four-step sequence for acquisition of offset-corrected potential difference $V_2 - V_1$.

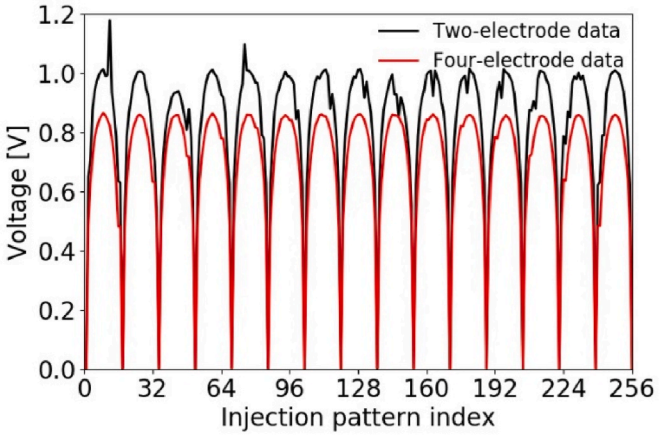

Fig. 7. Pseudo-periodical patterns obtained by plotting the measured potential difference against the injection pattern index defined as $16 \times (n - 1) + m$, where n and m ($1 \leq n, m \leq 16$) are the unit indices of negative and positive injection/measurement electrodes, respectively.

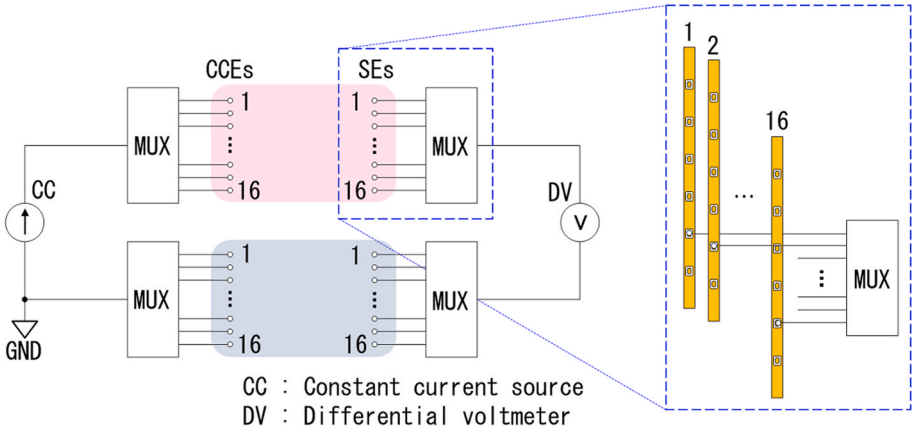

Fig. 5. Electrode connections. SEs in the second row from the bottom in each electrode unit are connected to MUXes.

unchanged.) The smooth and regular changes of the signal indicate that all the SEs were functioning well. Similarly, the two-electrode data (gray lines) indicate that all the CCEs were functioning well too. The data, however, show irregular changes in addition to the extra potential difference caused by the polarization of CCEs. The irregularities may not necessarily indicate surface contamination because the two-electrode data are affected by the injection history of the individual CCEs. This occurs because the response of CCEs to an injection pulse is dependent on the preexisting amount of charge in EDLs as discussed in Section 2.

4. Reconstruction of two-phase flow phantom

The performance of the present DC-driven design, characterized by measures for coping with electrode polarization, has been tested against experiments with varying levels of difficulty for reconstruction. Results from one of these cases are presented here with a focus on the effectiveness of the electrode design.

4.1. Experiment

A simple object shown in Fig. 8, consisting of two non-conductive, cylindrical inclusions in a homogeneous medium was used to obtain data for reconstructions. The inclusions were 18 mm diameter rods made of chloroethylene, and were placed in a rotationally asymmetric arrangement, one nearer the wall and the other nearer the center of a cylindrical vessel. (The two shorter rods seen on the photo (Fig. 8(c)) serve as a spacer which do not protrude into water.) The vessel was filled with tap water with a conductivity of 176 μS/cm to a depth of 85 mm. Data were taken by both four-electrode and two-electrode methods with a current amplitude of 500 μA with and without inclusions in the vessel.

Data taken with the adjacent-adjacent injection-measurement strategy are used for the reconstructions presented in this section. The adjacent injection strategy, when applied to the sixteen CCEs in the present design, produces sixteen different current patterns: (1 →2), (2 →3), …, (16 →1), where the numbers indicate unit IDs and the arrows indicate the directions of current. This injection strategy ensures that the injection into each CCE to be charge balanced.

The adjacent measurement strategy, when applied to the sixteen SEs in the present design, produces data from sixteen different adjacent pairs of SEs (1,2), (2,3), …, (16,1). Due to the compound electrode design, all the SEs are available for measurement irrespective of which CCEs are being used for injection. As a result of sixteen measurements for each of sixteen injection patterns, we obtain a total of 256 data for reconstruction.

4.2. Basic algorithm

The electric potential $\varphi(\boldsymbol{x})$ in a single substance follows the Laplace equation, provided that $\varphi(\boldsymbol{x})$ varies slowly enough for the quasi-static approximation to hold [25]:

$$\nabla \cdot [\sigma(\boldsymbol{x}) \nabla \varphi(\boldsymbol{x})] = 0, \tag{3}$$

where $\sigma(\boldsymbol{x})$ is the conductivity of the substance. For solving Eq. (3) for unknown $\sigma(\boldsymbol{x})$'inversely' from the known boundary conditions $\varphi(\boldsymbol{x_b}) = V(\boldsymbol{x_b})$ on SEs, we use the EIDORS (Electrical Impedance Tomography and Diffuse Optical Tomography Reconstruction Software) ver. 3.10 package [22,26]. We apply the Gauss-Newton algorithm in EIDORS[1] to obtain $\sigma(\boldsymbol{x})$ as an iterative solution of a least squares problem for. $V(\boldsymbol{x_b})$.

Each iteration step starts with a 'forward' prediction of $V(\boldsymbol{x_b})$ based on a current guess of $\sigma(\boldsymbol{x})$, with use of the finite element method (FEM). A residual function $f(\sigma(\boldsymbol{x_b}))$ is defined as the sum of the squared error of forward prediction $F(\sigma(\boldsymbol{x}))$ and a regularization term that includes a regularization matrix R and a positive parameter λ

$$f(\sigma(\boldsymbol{x_b})) = \frac{1}{2}||F(\sigma(\boldsymbol{x})) - V(\boldsymbol{x_b})||^2 + \frac{1}{2}\lambda^2||R\sigma(\boldsymbol{x})||^2. \tag{4}$$

We use discrete Laplacian filter available in EIDORS[2] for R, and a value of 0.01 for λ. If the residual function $f(\sigma(\boldsymbol{x_b}))$ has not converged to its minimum, then an updated guess of $\sigma(\boldsymbol{x})$ is defined for the next iteration step as

$$\sigma(\boldsymbol{x})_{k+1} = \sigma(\boldsymbol{x})_k + h_{GN}, \tag{5}$$

by using the correction term h_{GN} obtained inversely from the forward prediction error $(F(\sigma(\boldsymbol{x})) - V(\boldsymbol{x_b}))$:

$$\begin{aligned} h_{GN} \quad = \quad & \left(F'(\sigma(\boldsymbol{x}))^T F'(\sigma(\boldsymbol{x})) + \lambda^2 R^T R\right)^{-1} \\ & F'(\sigma(\boldsymbol{x}))^T (V(\boldsymbol{x_b}) - F(\sigma(\boldsymbol{x}))), \end{aligned} \tag{6}$$

where $F'(\sigma(\boldsymbol{x}))$ is the Jacobian matrix, $F'(\sigma(\boldsymbol{x}))^T$ is the transpose matrix of $F'(\sigma(\boldsymbol{x}))$.

4.3. Approach and methods for reconstruction

We choose the difference imaging approach [27,28] for the present problem because we are more interested in imaging of discontinuities, because of its relevance to two-phase flow measurements, than quantification of conductivity. To obtain the differential conductivity distribution $\delta\sigma(\boldsymbol{x})$ caused by the presence of inclusions, data taken with and without the inclusions are used. The differences between the two data sets $\delta V(\boldsymbol{x_b})$ are used for reconstruction with the difference imaging solver in EIDORS.

Reconstructions are done for a two-dimensional plane at the height of SEs 45 mm above the vessel bottom. A 2D mesh shown in Fig. 9 is used for both forward and inverse calculations. It is composed of 2123 nodes and 4060 triangle elements. The green arcs on the surface indicate the peripheral lengths covered by CCEs.

The boundary conditions on the electrode surfaces are given in EIDORS based on the so-called complete electrode model [22,29]:

$$V(\boldsymbol{x_b}) = \varphi(\boldsymbol{x_b}) + z_l \sigma(\boldsymbol{x_b}) \frac{\partial \varphi(\boldsymbol{x_b})}{\partial n}, \tag{7}$$

where z_l is the contact impedance, treated as a real number. Clearly, Eq. (7) considers AC injection, and z_l represents the electrode polarization impedance at the injection frequency. Eq. (7), specifically its second term in the right-hand side, is inapplicable to DC-driven electrodes. It however works in specifying $V(\boldsymbol{x_b})$ by using four-electrode data taken by SEs because the term in question equals to zero on SEs. The specification of z_l value, left to the user, can affect the quality of reconstructed images. Since Eq. (7) is applied to passive as well as active electrodes, the value of z_l would determine the magnitude of shunting current on passive CCEs discussed in Section 2.3, although the influence may become invisible when the difference imaging technique is applied. In the present reconstructions we tentatively used a fixed value of $z_l = 1.0$ ohm m, having found that the reconstructed images were insensitive to the value of z_l. In specification of $V(\boldsymbol{x_b})$, each electrode unit, 6 mm in width, was assumed to have a uniform potential $V(\boldsymbol{x_b})$ for simplicity.

4.4. Results

Fig. 10 (a) and (b) show the relative conductivity maps reconstructed from the four- and two-electrode data, respectively. Although the two results may not look much different at a glance, in the two-electrode case (b) the cylinder on the left is reconstructed in a distorted form, and large fluctuations are seen over the entire image. Furthermore, a red "ghost"

[1] Option "inv_solve_gn" is selected as the variable "solve".

[2] Option "prior_laplace" is selected as the variable "RtR_prior".

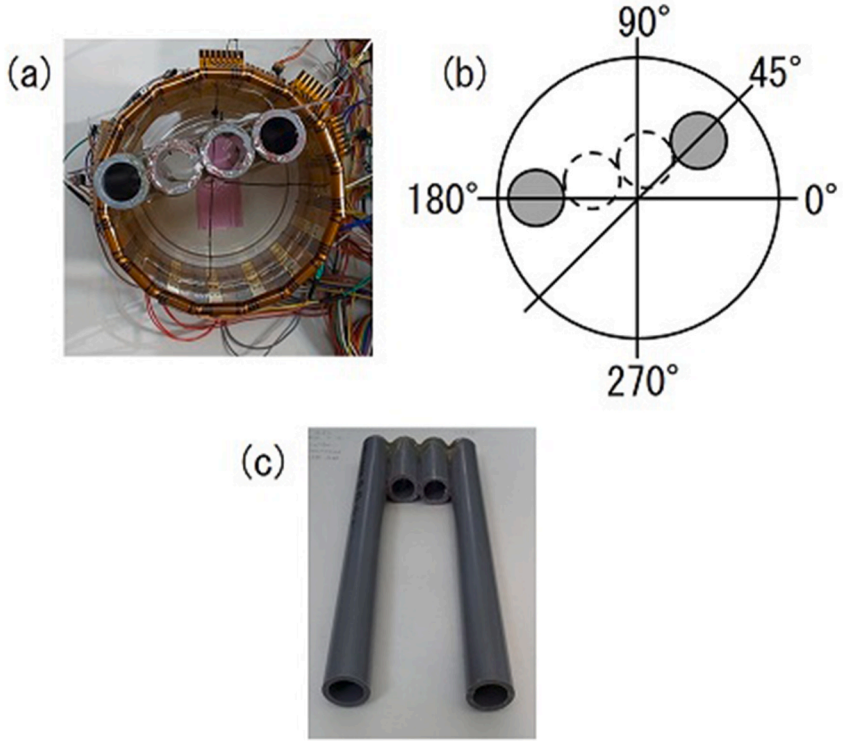

Fig. 8. (a) A top view photo of EIT experimental system. It is flipped horizontally because the indices of electrodes are in reverse order between the experimental system and analysis models. (b) Schematic diagram of two rods arrangement in 2D plane. The gray circles are the location of rods. (c) The photo of the hollow rods.

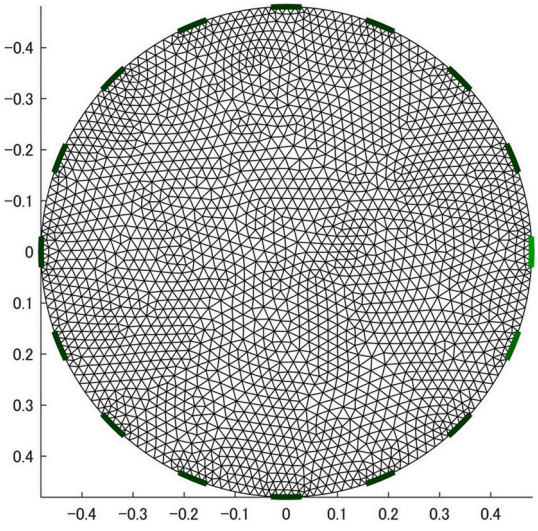

Fig. 9. The 2D mesh for FEM. Green arcs on the boundary represent the peripheral lengths covered by electrodes. (Unit: 10 cm).

appears near the lower-left wall in (b).

The limitations of the two-electrode method are now evident despite that the limitations are mitigated in the present design by the use of a constant current source and a charge-balanced injection strategy. The results presented so far show that the four-electrode measurement, based on a compound electrode design and the use of a stable constant current source, can provide reliable data essentially unaffected by the polarization of CCEs in a DC-driven EIT system.

5. Conclusions

A DC-driven EIT system, based on boundary measurement of potential difference response to pulsed-DC injection, has been developed for imaging of gas/water two phase flow. Major problems encountered and the solutions adopted can be summarized as follows.

- DC-driven electrodes are polarized to indicate an extra, drifting potential difference that can be comparable to the ohmic potential difference to be measured for image reconstruction. The influence of extra component on measurement needs to be limited or corrected for. The present design uses dedicated electrodes for injection and measurement to eliminate the influence.
- The extra potential difference prompts faradaic reactions involving water impurities. The reactions can cause electrode surface contamination and alter the ionic environment of electrodes. The present design uses injection amplitude and pulse width chosen appropriately to obtain ohmic potential difference large enough for accurate measurement while limiting the rate of faradaic reactions and preventing water electrolysis on the injecting electrodes.

The DC-driven EIT system presented in this paper is characterized by its simple and flexible configuration composed of easily available analogue components. Improvements for better spatial resolution and higher measurement speed are now planned for enhanced applicability to two-phase flow measurements.

Authorship contributions

Yoshiyasu Hirose: Formal analysis, Software, Visualization, Writing - original draft. Jun Sagawa: Conceptualization, Methodology, Gathering experimental data, Validation. Yasuteru Sibamoto: Supervision, Writing - review & editing. Yutaka Kukita: Conceptualization, Methodology, Supervision, Writing - original draft.

Declaration of competing interest

The authors declare that they have no known competing financial

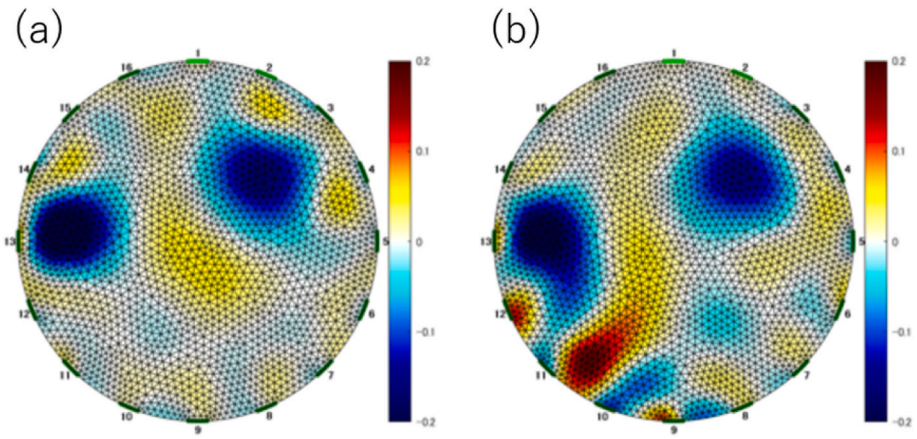

Fig. 10. Reconstructed relative conductivity map based on four-electrode data (a) and two-electrode data (b).

interests or personal relationships that could have appeared to influence the work reported in this paper.

Appendix A. Influence of conductive surfaces on the response of potential difference to current injection

The influence of conducting surfaces on the response of potential difference to current injection was studied for different geometries, frequencies (1–10,000 Hz) and current waveforms (square and sinusoidal). The electrode units described in Section 2.1 were used with different arrangements of conducting surfaces relative to the current flow path between the CCEs as summarized in Table A1 and shown in Fig. A1. The "EIT geometry" experiment used adjacent-but-one injection-measurement configuration in the EIT test vessel shown in Fig. 2. Case 1 through 3 experiments used a rectangular vessel with and without a passive unit or a conductive inclusion placed between active units that were more closely spaced than in the EIT geometry.

Four-electrode measurement results for 100 Hz square wave injection are presented in Fig. A2. The Case 1 and EIT-geometry results show small overshoots at the leading edge, while Case 2 and Case 3, with enhanced interactions between the current flow and the conductive surfaces, show rounding at the leading edge characteristic of capacitive influence.

Table A.1
Experimental conditions

	Distance (mm)	Number of passive units	Conductive inclusion
EIT Geometry	26 (adjacent but one)	14	–
Case 1	16	–	–
Case 2	16	1	–
Case 3	16	–	20 mm wide aluminum plate, 5 mm apart from electrode surfaces

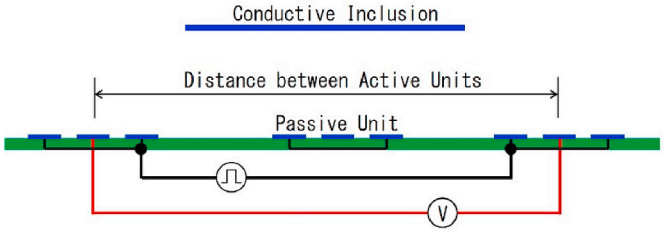

Fig. A.1. Experimental geometry. The current source is connected to CCEs in each electrode unit through MUXes. The voltmeter circuit is connected to the SEs in the second row from the bottom in each electrode unit through MUXes.

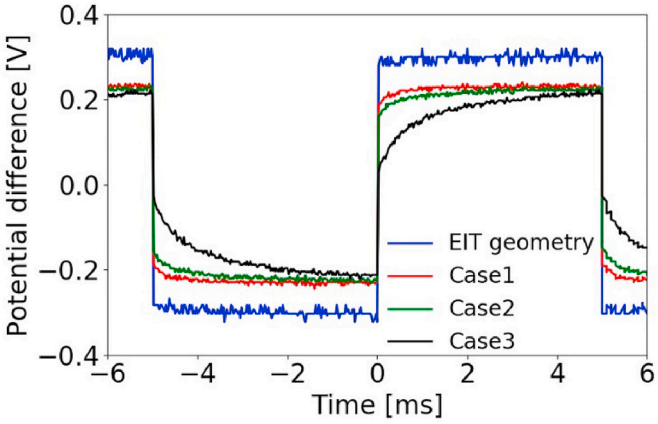

Fig. A.2. Potential difference signals obtained for 100 Hz square wave current injection for different geometries.

References

[1] L. Borcea, Electrical impedance tomography, Inverse Probl. 18 (2002) R99–R136.
[2] Available at: https://www.leeds.ac.uk/olil/tomography/EIT.php. (Accessed 1 March 2021).
[3] W. Yan, S. Hong, R. Chaoshi, Optimum design of electrode structure and parameters in electrical impedance tomography, Physiol. Meas. 27 (3) (2006 Mar) 291–306, https://doi.org/10.1088/0967-3334/27/3/007. Epub 2006 Feb 1. PMID: 16462015.
[4] Y. Wang, S. Ren, F. Dong, Focusing sensor design for open electrical impedance tomography based on shape conformal transformation, Sensors 19 (9) (2019) 2060, https://doi.org/10.3390/s19092060.
[5] C. Tan, S. Lv, F. Dong, M. Takei, Image reconstruction based on convolutional neural network for electrical resistance tomography, IEEE Sensor. J. 19 (1) (2019) 196–204, https://doi.org/10.1109/JSEN.2018.2876411, 1 Jan.1.
[6] A. Adler, J.H. Arnold, R. Bayford, A. Borsic, B. Brown, P. Dixon, T.J. Faes, I. Frerichs, H. Gagnon, Y. Gärber, B. Grychtol, G. Hahn, W.R. Lionheart, A. Malik, R.P. Patterson, J. Stocks, A. Tizzard, N. Weiler, G.K. Wolf, GREIT: a unified approach to 2D linear EIT reconstruction of lung images, Physiol. Meas. 30 (6) (2009 Jun) S35–S55, https://doi.org/10.1088/0967-3334/30/6/S03. Epub 2009 Jun 2. PMID: 19491438.
[7] S. Friedel, A. Thielen, S.M. Springman, Investigation of a slope endangered by rainfall-induced landslides using 3D resistivity tomography and geotechnical testing, J. Appl. Geophys. 60 (Issue 2) (2006) 100–114, https://doi.org/10.1016/j.jappgeo.2006.01.001. ISSN 0926-9851.
[8] Danny Smyl, Electrical tomography for characterizing transport properties in cement-based materials: a review, Construct. Build. Mater. 244 (2020) 118299, https://doi.org/10.1016/j.conbuildmat.2020.118299. ISSN 0950-0618.
[9] Feng Dong, Xiaoping Liu, Xiang Deng, Lijun Xu, Ling-an Xu, Identification of two-phase flow regimes in horizontal, inclined and vertical pipes, Meas. Sci. Technol. 12 (2001) 1069.
[10] M. Wang, W. Yin, N. Holliday, A highly adaptive electrical impedance sensing system for flow measurement, Meas. Sci. Technol. 13 (2002) 1884.
[11] M. Darnajou, A. Dupré, C. Dang, G. Ricciardi, S. Bourennane, C. Bellis, S. Mylvaganam, High speed EIT with multifrequency excitation using FPGA and response analysis using FDM, IEEE Sensor. J. 20 (15) (2020) 8698–8710, https://doi.org/10.1109/JSEN.2020.2984388, 1 Aug.1.
[12] Q. Wang, B. Karki, Y. Faraj, M. Wang, Improving spatial and temporal resolution of electrical impedance tomogram (EIT) by partial imaging with limited measurements (PILM), in: Proc. 7th Int. Symp. On Process Tomography, Dresden, Germany, 1–3 September, 2015.
[13] A. Dupré, S. Mylvaganam, A simultaneous and continuous excitation method for high-speed electrical impedance tomography with reduced transients and noise sensitivity, Sensors 18 (4) (2018) 1013, https://doi.org/10.3390/s18041013.
[14] J. Padilha Leitzke, H. Zangl, A review on electrical impedance tomography spectroscopy, Sensors 20 (18) (2020) 5160, https://doi.org/10.3390/s20185160.
[15] Torleif Dahlin, Virginie Leroux, Johan Nissen, Measuring techniques in induced polarisation imaging, J. Appl. Geophys. 50 (Issue 3) (2002) 279–298, https://doi.org/10.1016/S0926-9851(02)00148-9. ISSN 0926-9851.
[16] A.J. Wilkinson, E.W. Randall, J.J. Cilliers, D.R. Durrett, T. Naidoo, T. Long, A 1000-measurement frames/second ERT data capture system with real-time visualization, IEEE Sensor. J. 5 (2) (April 2005) 300–307, https://doi.org/10.1109/JSEN.2004.842445.
[17] Herman P. Schwan, Clifford D. Ferris, Four-electrode null techniques for impedance measurement with high resolution, Rev. Sci. Instrum. 39 (1968) 481, https://doi.org/10.1063/1.1683413.
[18] T. Vilhunen, J.P. Kaipio, P.J. Vauhkonen, T. Savolainen, M. Vauhkonen, Simultaneous reconstruction of electrode contact impedances and internal electrical properties: I. Theory, Meas. Sci. Technol. 13 (2002) 1848.
[19] Peter James Lingane, Dennis G. Peters, Chronopotentiometry, CRC Crit. Rev. Anal. Chem. 1 (4) (1971) 587–634, https://doi.org/10.1080/1040834nu08542742.
[20] Yulia Polevaya, Irina Ermolina, Michael Schlesinger, Ben-Zion Ginzburg, Yuri Feldman, Time domain dielectric spectroscopy study of human cells: II. Normal and malignant white blood cells, Biochim. Biophys. Acta Biomembr. 1419 (Issue 2) (1999) 257–271, https://doi.org/10.1016/S0005-2736(99)00072-3. ISSN 0005-2736.
[21] Yu Feldman, E. Polygalov, I. Ermolina, Polevaya Yu, B. Tsentsiper, Electrode polarization correction in time domain dielectric spectroscopy, Meas. Sci. Technol. 12 (2001) 1355.
[22] Nick Polydorides, William R.B. Lionheart, A Matlab toolkit for three-dimensional electrical impedance tomography: a contribution to the Electrical Impedance and Diffuse Optical Reconstruction Software project, Meas. Sci. Technol. 13 (2002) 1871.
[23] L. Feng, Q. Li, S.D. Cameron, et al., Quantifying induced polarization of conductive inclusions in porous media and implications for geophysical measurements, Sci. Rep. 10 (2020) 1669, https://doi.org/10.1038/s41598-020-58390-z.
[24] M. Wang, Y. Ma, Over-zero switching scheme for fast data collection operation in electrical impedance tomography, Meas. Sci. Technol. 17 (2006) 2078.
[25] M. Cheney, D. Isaacson, J. Newell, Electrical impedance tomography, SIAM Rev. 41 (1) (1999) 85–101, https://doi.org/10.1137/S0036144598333613. Retrieved March 2, 2021.
[26] Available at: http://eidors3d.sourceforge.net/. (Accessed 1 March 2021).
[27] liu Dong, Ville Kolehmainen, Samuli Siltanen, Anne-maria Laukkanen, Seppänen Aku, Estimation of conductivity changes in a region of interest with electrical impedance tomography, Inverse Probl. Imag. 9 (1) (2015) 211–229, https://doi.org/10.3934/ipi.2015.9.211.
[28] A.K. Khambampati, D. Liu, S.K. Konki, K.Y. Kim, An automatic detection of the ROI using otsu thresholding in nonlinear difference EIT imaging, IEEE Sensor. J. 18 (12) (2018) 5133–5142, https://doi.org/10.1109/JSEN.2018.2828312, 15 June15.
[29] W. Chen, J. Cheng, J. Lin, et al., A level set method to reconstruct the discontinuity of the conductivity in EIT, Sci. China Ser. A-Math. 52 (2009) 29–44, https://doi.org/10.1007/s11425-008-0156-2.